Electronic Supplementary Material (ESI) for Reaction Chemistry & Engineering.
This journal is © The Royal Society of Chemistry 2019

Electronic Supplementary Information

Continuous Generation, In-line Quantification and Utilization of Nitrosyl Chloride in Photonitrosation Reactions

René Lebl,[a,b] David Cantillo*[a,b] and C. Oliver Kappe*[a,b]

[a] Center for Continuous Flow Synthesis and Processing (CC FLOW), Research Center Pharmaceutical Engineering GmbH (RCPE), Inffeldgasse 13, Graz, Austria

[b] Institute of Chemistry, University of Graz, Heinrichstrasse 28, 8010 Graz, Austria.

Email: david.cantillo@uni-graz.at, oliver.kappe@uni-graz.at

Table of Contents

1 Development of the NOCl Generator S2
1.1 UV/Vis analysis of NOCl S2
1.2 Implementation of a UV/Vis flow cell S3
1.3 Optimization of NOCl generation in flow S5
1.4 Determination of the NOCl amount by redox titration S10
2 Development of a telescoped photoreaction S10
2.1 Photoreactor for preliminary experiments S10
2.2 Implementation of a Corning photoreactor S11
2.3 Optimization of the photoreaction S12
2.4 Characterization of cyclohexanone oxime S14
3 References S14
4 NMR spectra S15

1 Development of the NOCl Generator

1.1 UV/Vis analysis of NOCl

To obtain reference spectra of NOCl in solution, NOCl was generated within the organic solvent from isoamyl nitrite ($C_5H_{11}ONO$) and chlorotrimethylsilane (TMSCl) according to Scheme S1.[S1–S3] For initial experiments increasing amounts of TMSCl were added stepwise to a solution of $C_5H_{11}ONO$ in $CHCl_3$.

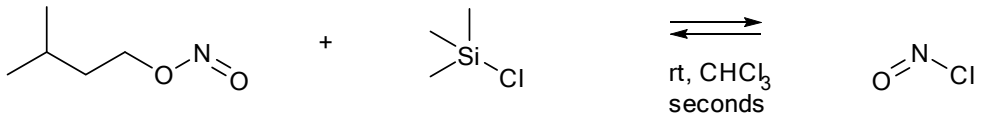

Scheme S1 Formation of nitrosyl chloride within an organic solvent.

In a 10 mm quartz cuvette, a 0.4 M solution $C_5H_{11}ONO$ in $CHCl_3$ was treated with 0.25 equiv. TMSCl at ambient temperature. While a magnetic stir bar at the bottom of the cuvette ensured sufficient mixing, two independent absorption spectra were recorded at 0 min and 5 min after the addition of TMSCl. This procedure was repeated until the amount of TMSCl corresponded 2 equiv. relative to $C_5H_{11}ONO$. Since no time dependent difference of the absorbance at 472 nm and 583 nm within the 5 min intervals could be observed, we concluded a fast adjustment of the equilibrium state for the NOCl formation. Further amounts of TMSCl were added to the solution. The observed absorbance for NOCl did not increase after 4 equiv TMSCl had been added.

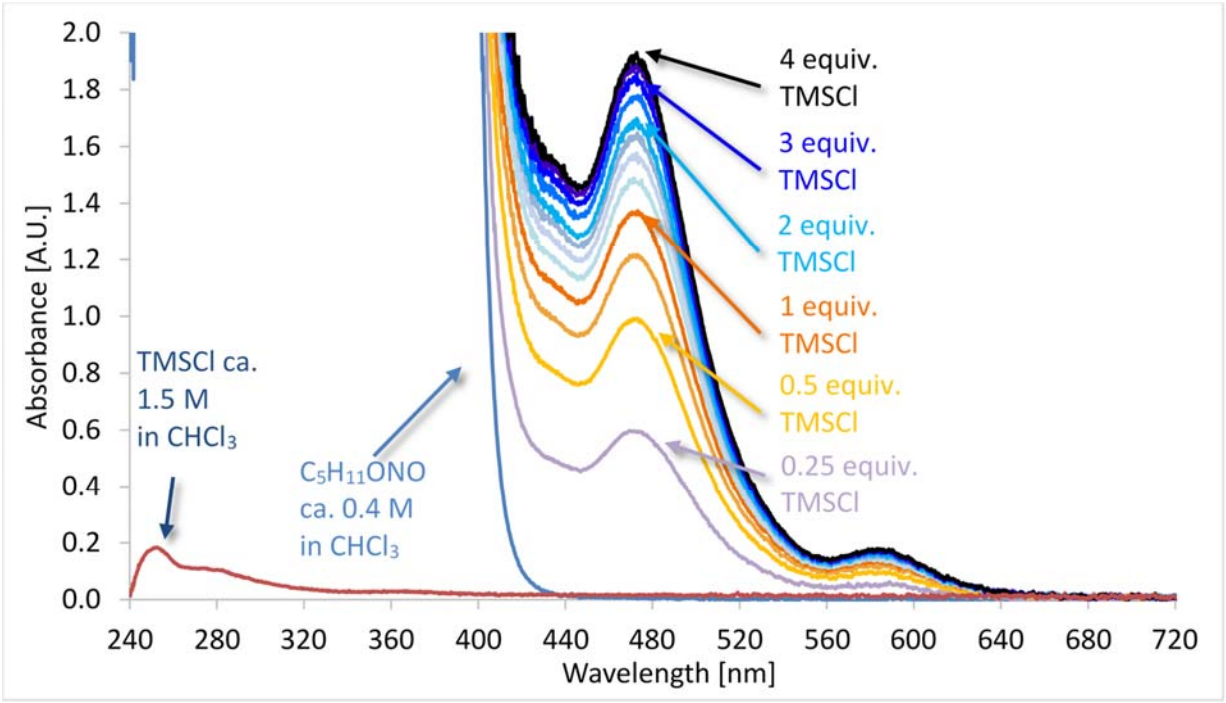

Fig. S1 Absorbance of nitrosyl chloride in chloroform, formed from $C_5H_{11}ONO$ and TMSCl.

Based on these results we assumed to quantitative conversion of isoamyl nitrite to NOCl upon the addition of 4 equiv. of TMSCl within seconds. To estimate the concentration depended absorbance of nitrosyl chloride in chloroform at 472 nm and 583 nm, we measured 7 stock solutions and a blank sample. The two resulting calibration curves in Fig. S2 linearly correlate and provide a good basis to estimate the concentration of nitrosyl chloride within an organic solvent. Since we were expecting a concentration between 0.5 M and 1.0 M, we decided to follow the local absorption maximum at 583 nm exclusively throughout the following optimizations, as the absorbance at 472 nm measured by a 10 mm quartz cuvette exceeds the optimal range of the spectrometer.

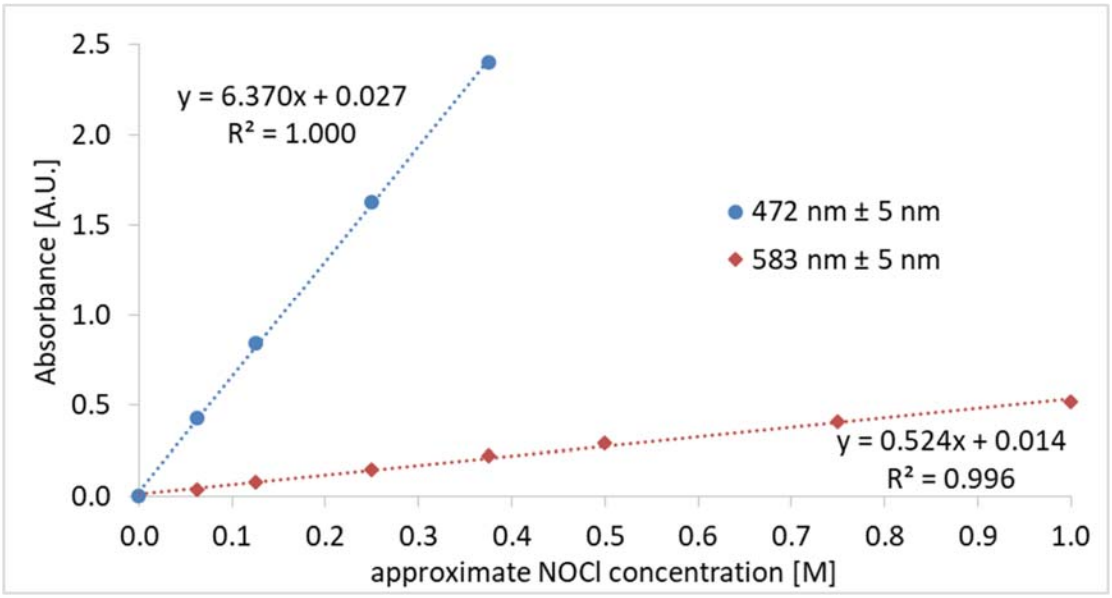

Fig. S2 Correlation between approximate nitrosyl chloride concentration and absorbance at 472 nm and 583 nm.

1.2 Implementation of a UV/Vis flow cell

The absorption properties of two fluorinated ethylene propylene (FEP) films, with a different thickness of 0.25 mm and 0.05 mm were examined to ensure no interference with the absorption measurements, when they were used as protective layer between the tips of the optical probes and the solvent stream containing NOCl. The absorption spectra of two 0.25 mm films and two 0.05 mm films are shown in Fig. S3 and exhibit high transparency for the visible region. For two films with a thickness of 0.05 mm, we found a low absorbance (less than 0.2 A.U.) down to a wavelength of 250 nm. Since in the range of special interest for our application, around 583 nm, the transmission of 0.05 mm FEP films is greater than 90%, they were selected for the implementation in the flow cell, as the remaining background could be easily be compensated by blank references.

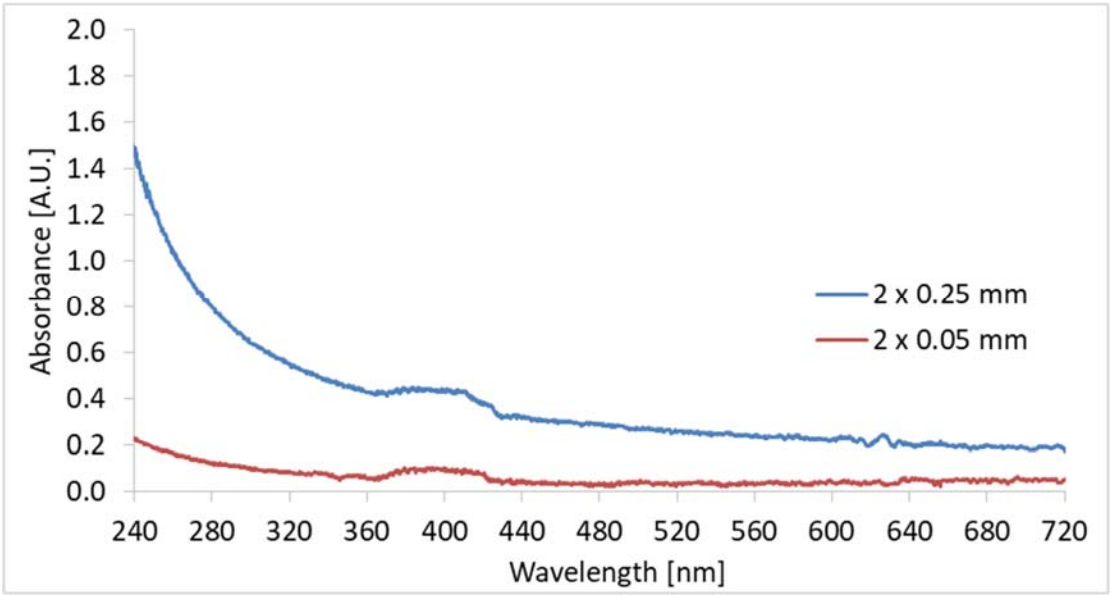

Fig. S3 UV/Vis absorption of fluorinated ethylene propylene sheets.

Next, we removed the stainless steel coated optical probes from both sides of the flow cell, and left the FEP films with a thickness of 0.05 mm clamped between the ¼-28 flat bottom fittings and the cell to test their mechanical robustness. We gradually applied a back pressure up to 14 bar to the system, but could not observe any rupture or breakthrough of the solvent. Eventually only a small dent in the FEP film was visible when the FEP film was recovered after the experiments, as shown in Fig. S4.

Fig. S4 FEP film with a thickness of 0.05 mm after mechanical stress test.

Ultimately, the flow cell was evaluated by comparing an absorption spectrum of an isoamyl nitrite solution 10 mM in $CHCl_3$ measured in a 10 mm quartz cuvette to the spectrum of the same solution recorded by using the flow cell (Fig. S5).

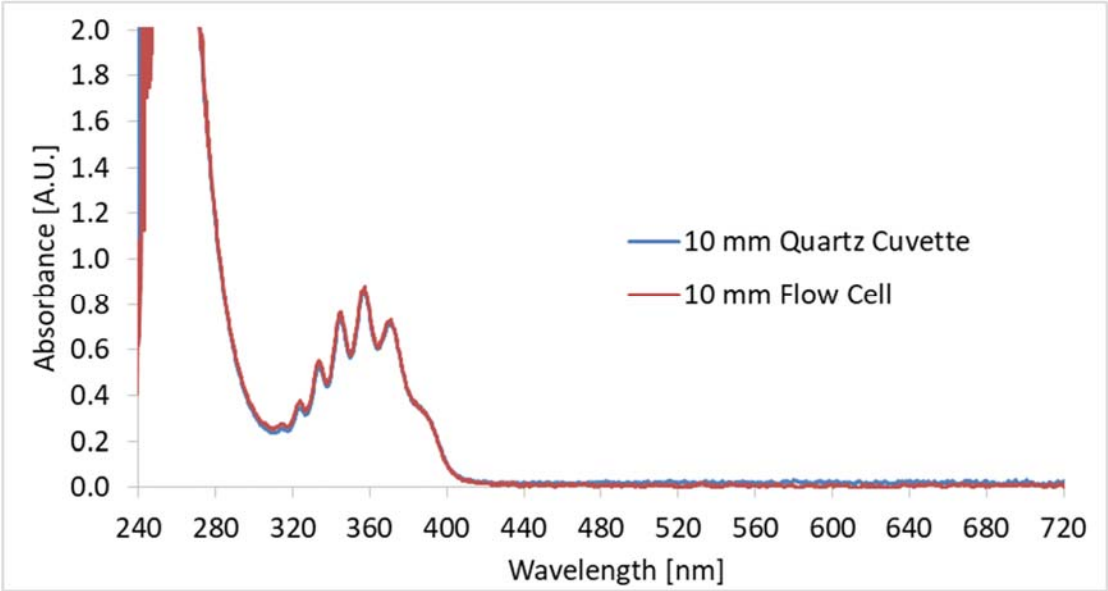

Fig. S5 Isoamyl nitrite absorption: flow cell compared to a quartz cuvette.

1.3 Optimization of NOCl generation in flow

The initial optimization of the NOCl generation in flow focussed on the determination of the necessary equivalents of HCl over $NaNO_2$. For these experiments, the flow setup according to Fig. 1 was used. The flow rate of the HCl stream (6 M aqueous solution) was varied, while maintaining a constant flow rate for $CHCl_3$ (400 µL/min) and for $NaNO_2$ 8 M in H_2O (50 µL/min). The UV/Vis absorption for the characteristic maximum of NOCl at 583 nm was continuously monitored in-line over time, while the different conditions were screened. For an easy comparison of the obtained data, the different plateaus during each "steady state" were averaged and plotted in Fig. S6. Conditions employing less than 4 equivalents of HCl caused the formation of gas slugs which did not allow for stable UV/Vis absorption measurements. According to Fig. S6 a plateau was reached when using 6 equivalents HCl or more, corresponding to an HCl flow rate of 400 µL/min. Thus, 6 equiv of HCl were utilized for further experiments.

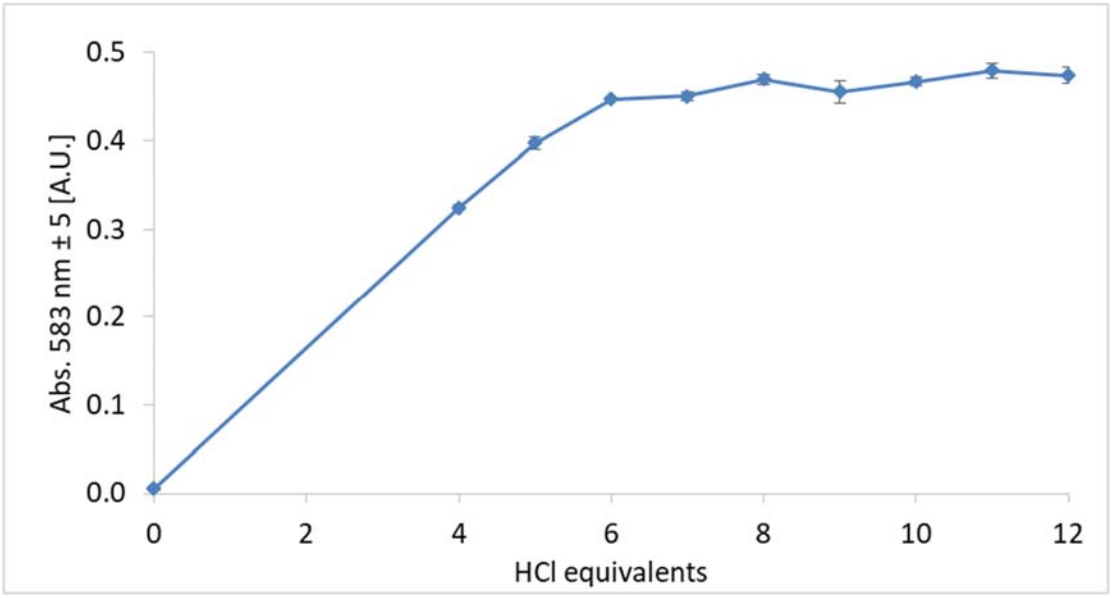

Fig. S6 Determination of HCl equivalents by in-line UV/Vis measurements.

We next investigated the influence of the ratio between the organic flow rate and the combined aqueous phases. Therefore, 16 different conditions were varied in approximately 15 min intervals, while the UV/Vis absorption of the resulting organic stream was monitored over time. In Fig. S7 the distinct transition between the various steady states be easily recognized.

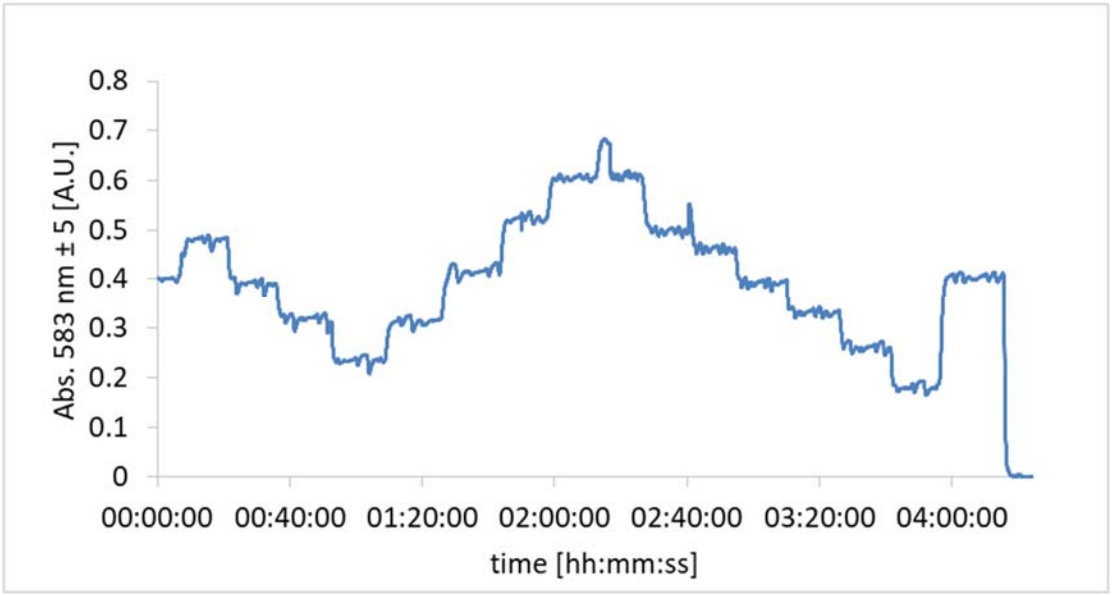

Fig. S7 Time dependent absorption during flow rate optimizations.

The different absorbance values at 583 nm, which were measured by applying 16 possible combinations between four organic and four aqueous flow rates were averaged and plotted in a three-dimensional bar chart in Fig. S8. The obtained values needed to be compensated for their theoretical NOCl yield, as higher aqueous flow rates and lower $CHCl_3$ flow rates automatically lead to an increased concentration of extracted nitrosyl chloride. In Fig.4, they were normalized to compare the actual extraction efficiency.

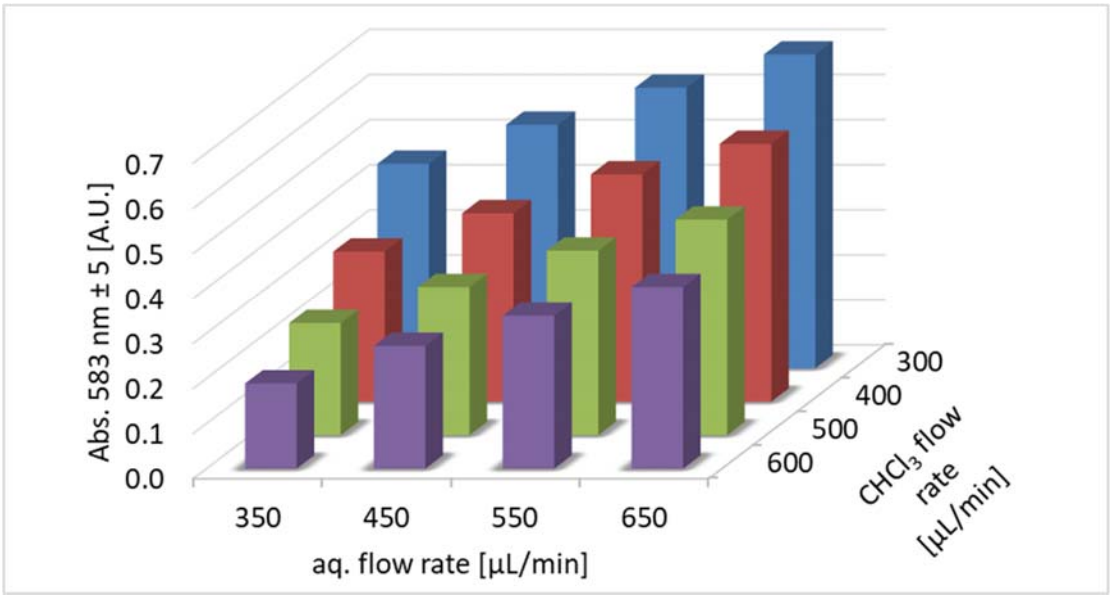

Fig. S8 Raw absorbance at 583 nm measured for the optimization of the ratio between organic and aqueous flow rates.

The relative NOCl yields displayed in Fig. 4, which is based on the normalized absorbance at 583 nm, were fitted to a 3rd order polynomial function, resulting in eqn. 1 with an R^2 coefficient of 0.9917.

$$z(x,y) = -0.425241 + 0.00261334\,x - 4.1962 \times 10^{-6}\,x^2 + 2.38883 \times 10^{-9}\,x^3 + \frac{2.02845 \times 10^7}{y^3} - \frac{116\,440}{y^2} - \frac{80.6333\,x}{y^2} + \frac{391.706}{y} - \frac{0.102698\,x}{y} + \frac{0.000142409\,x^2}{y} \quad (1)$$

When the surface corresponding to eqn. 1 z(x,y) is plotted in a contour map (Fig. S9), the conditions giving a high extraction efficiency can be recognized as bright orange regions in Fig. S9 due to the higher absorbance of NOCl at λ 583 nm. In contrast, conditions resulting in poor relative NOCl yield, especially in the corners (300,650) and (600,350), are depicted as dark blue regions in Fig. S9.

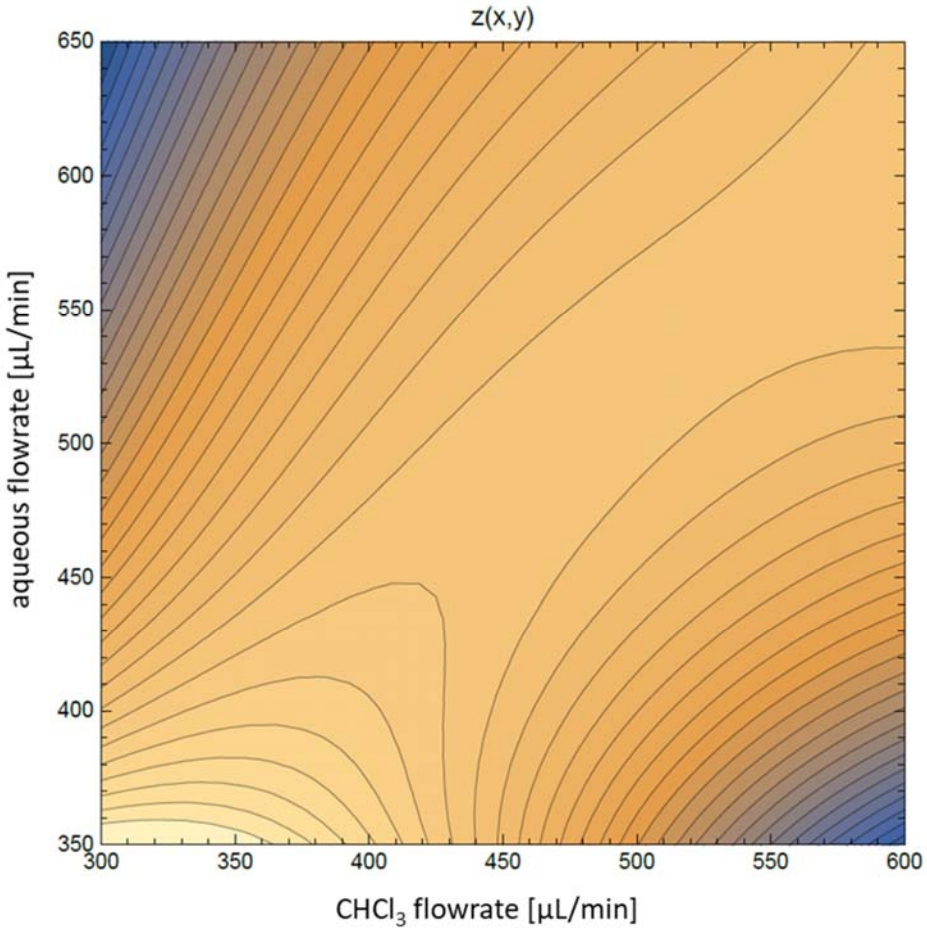

Fig. S9 Contour map for the surface corresponding to eqn. 1 z(x,y) with the x-axis representing the $CHCl_3$ flow rate [µL/min] and the y-axis representing the combined aqueous flow rate [µL/min].

To visualize the ridge line of this surface (Fig. S9), representing the conditions for higher relative NOCl yield across different total flow rates, the local direction of the gradient vector ∇z(x,y) was plotted in Fig. S10. The corresponding gradient vector is described in eqn. 2.

$$\nabla z(x,y) = \left\{0.00261334 - 8.3924 \times 10^{-6}\, x + 7.16649 \times 10^{-9}\, x^2 - \frac{80.6333}{y^2} - \frac{0.102698}{y} + \frac{0.000284818\, x}{y}, -\frac{6.08535 \times 10^{7}}{y^4} + \frac{232879}{y^3} - \frac{161.267\, x}{y^3} - \frac{391.706}{y^2} - \frac{0.102698\, x}{y} + \frac{0.000142409\, x^2}{y}\right\} \quad (2)$$

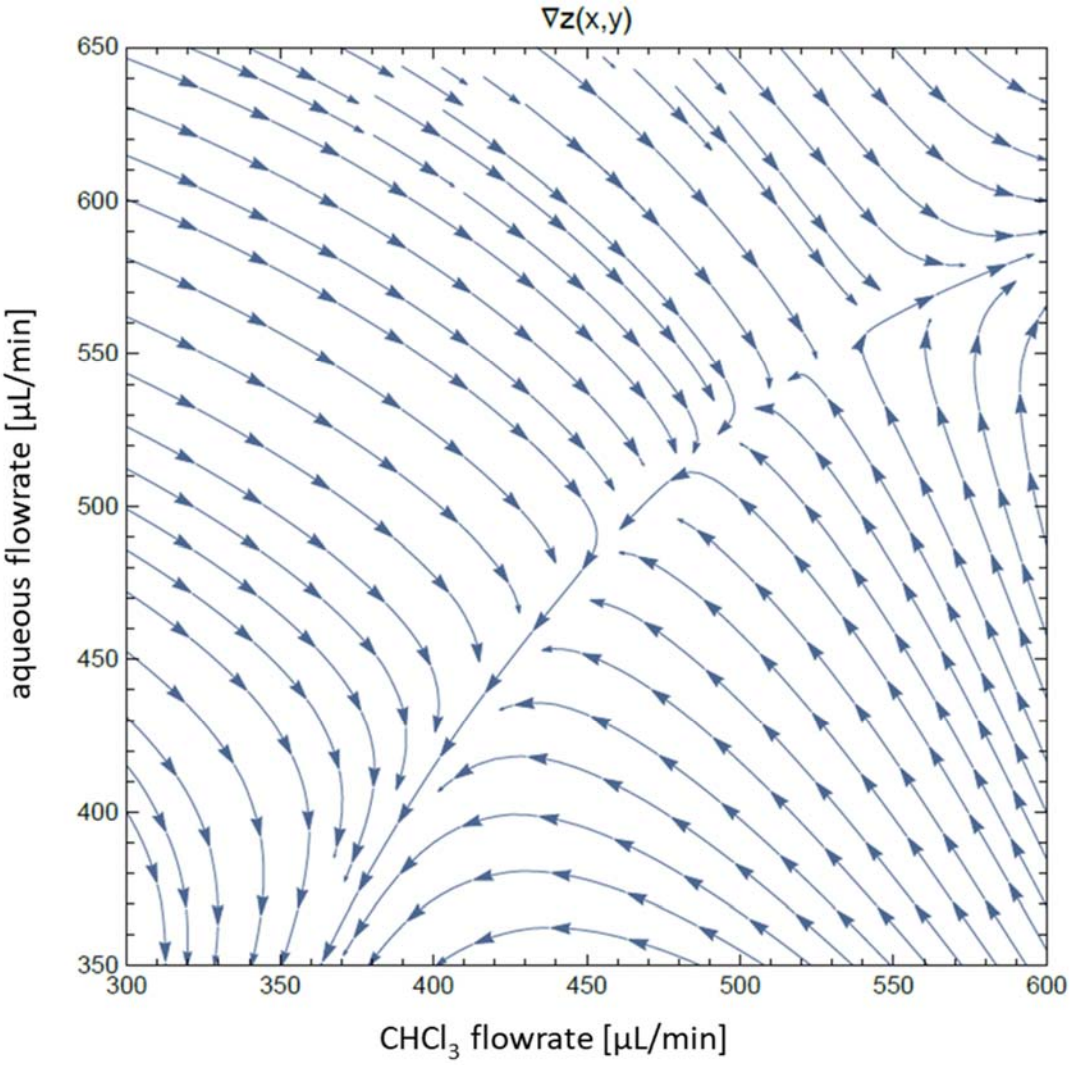

Fig. S10 Direction of the gradient vector (∇z(x,y)) at each point of the (x,y) plane.

The influence of the overall flow rate was investigated by measuring the absorption at 583 nm depending on 10 different settings. While the optimal flow rate ratio for $CHCl_3$, HCl (6 M) and $NaNO_2$ (8 M) was determined to be 9:8:1, the overall rate was varied between 200 µL/min and 2.00 mL/min, considering that specific ratio. The results depicted in Fig. S11 indicate only minor dependence of the NOCl generation and extraction performance on the overall flow rate. The relative standard deviation of all 10 absorbance values lies within 5%. These observations are beneficial for establishing a telescoped process in which the downstream reaction is more dependent on a specific flow rate and the residence time.

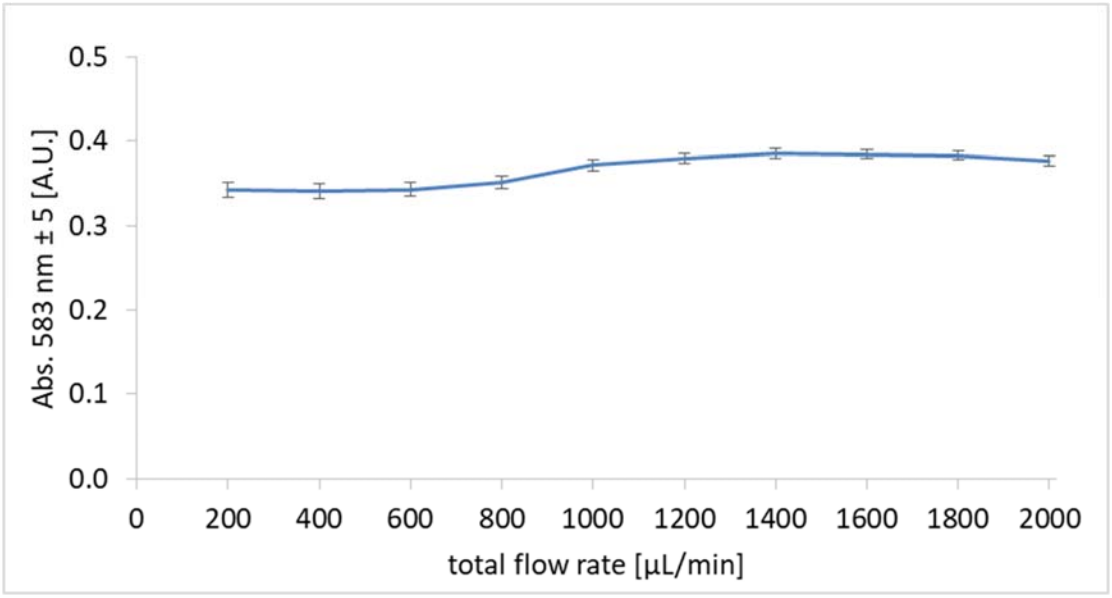

Fig. S11 Overall flow rate screening for the generation of NOCl.

1.4 Determination of the NOCl amount by redox titration

To unequivocally determine the amount of NOCl produced by the continuous generator under optimal conditions, a redox titration using the KI/I_2-$Na_2S_2O_3$ system was utilized.[S4] Thus, using the flow conditions described above, the organic stream from the reactor output was collected in a flask containing 50 mL of a 0.5 M aqueous solution of potassium iodide under stirring. Collection was extended for 10 min, corresponding to a theoretical amount of 5.4 mmol of NOCl. The resulting I_2 solution was titrated a standard 0.2 M solution of $Na_2S_2O_3$ using a burette. Determination was performed in triplicate.

2 Development of a telescoped photoreaction

2.1 Photoreactor for preliminary experiments

The eventual formation of precipitate and temperature dependence for the photonitrosation of cyclohexane were examined using a simple self-made photoreactor based on 0.8 mm ID PFA tubing. The coil with a total volume of 5.0 mL was wrapped around a tempering beaker (see Fig. S12). An additional aluminum layer helped to reflect the light internally, and a thermal insulation layer helped to control the temperature and prevented major condensation of water at low temperatures. The temperature was regulated by a minichiller 240 from Huber Kältemaschinenbau, and an additional temperature probe was installed at the bottom of the reactor. The photoreactor was illuminated from the top using a 50 W LED panel (λ_{max} = 455 nm).

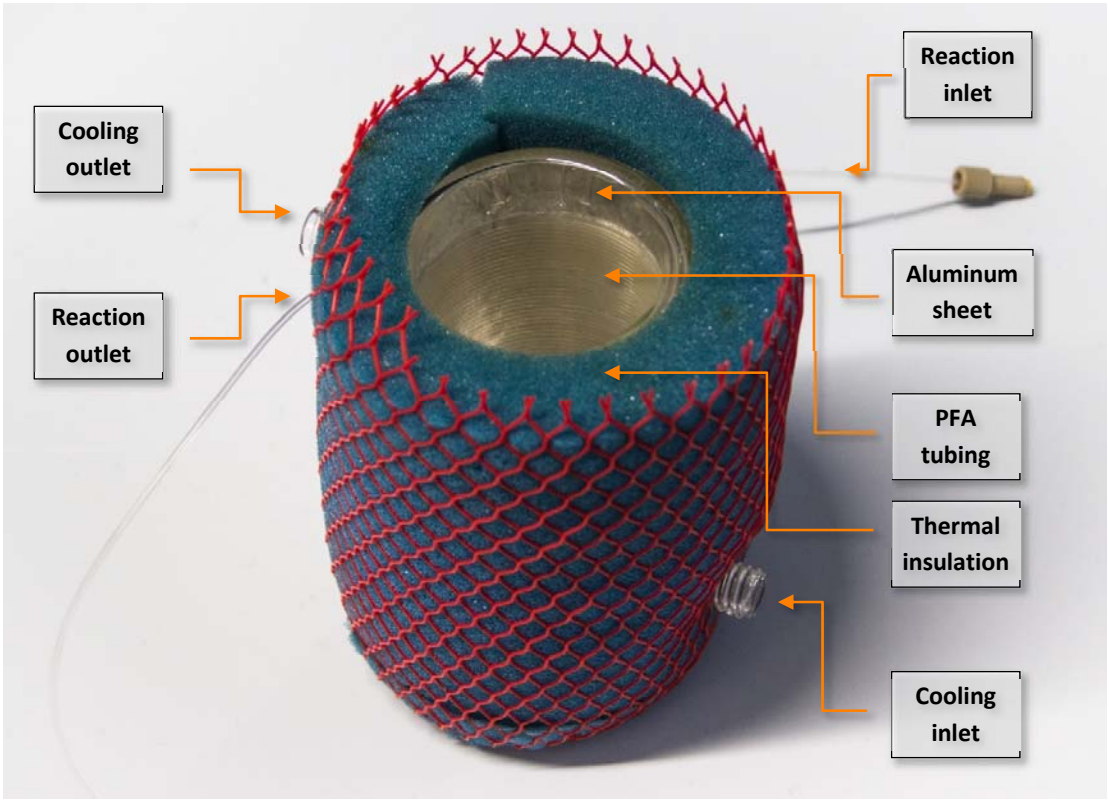

Fig. S12 Photoreactor for preliminary experiments.

2.2 Implementation of a Corning photoreactor

For the photonitrosation of cyclohexane performed in a Lab Photo Reactor from Corning, the setup depicted in Fig. S13 was used. The LED array was cooled to a constant temperature of 15 °C using a minichiller 280 from Huber Kältemaschinenbau. The temperature within the photo reactor was controlled by a Huber ministat 230. When no product was collected, especially during start-up and shut-down, the collection flask contained saturated aqueous $NaHCO_3$ to quench excess reagent. The substrate, cyclohexane, was mixed with the $NOCl/CH_2Cl_2$ stream immediately before entering the cooled reactor, to prevent freezing.

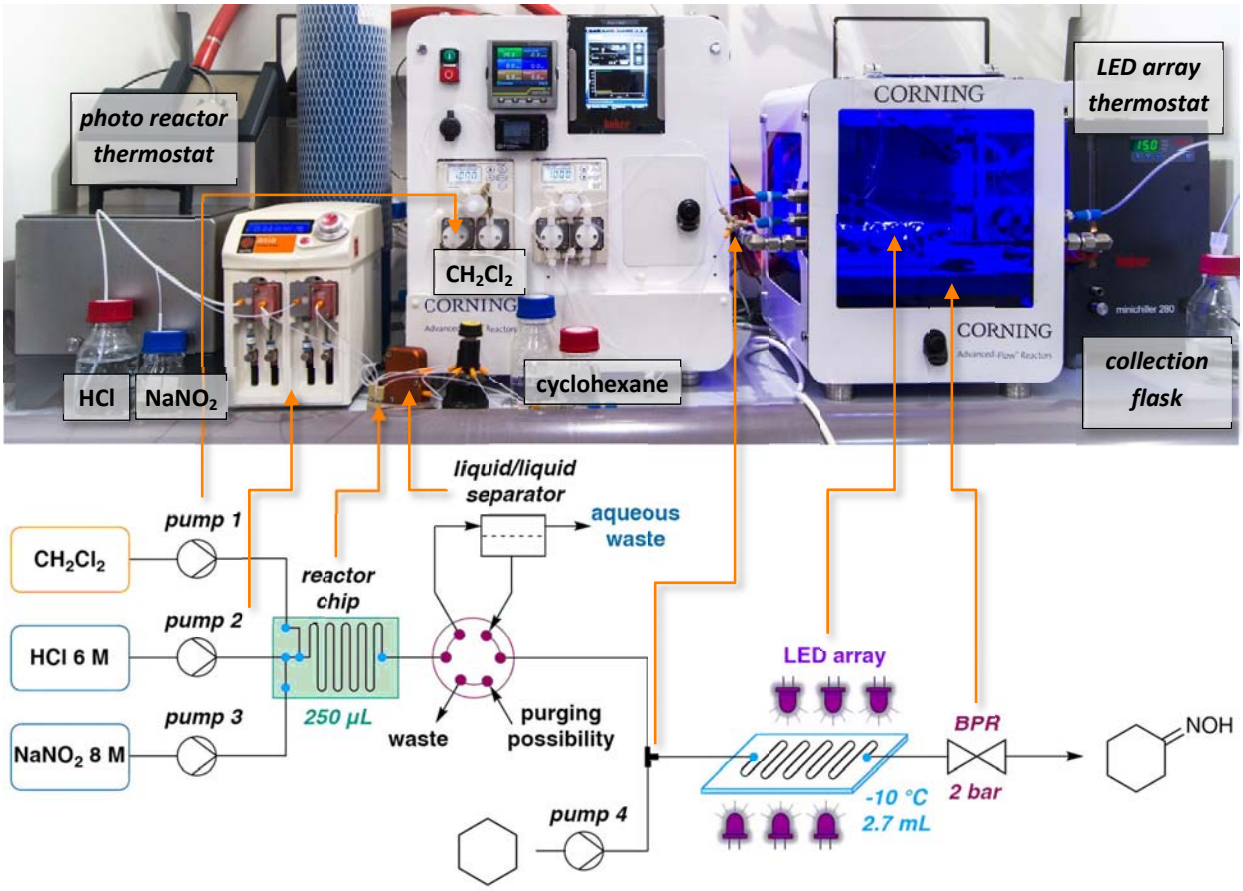

Fig. S13 Setup of the NOCl generation with a telescoped photoreaction.

2.3 Optimization of the photoreaction

To quantify the cyclohexanone by GC-FID, we decided to use diphenyl ether (Ph_2O) as internal standard (IS) and made a calibration with varying cyclohexanone oxime amounts accordingly. The calibration curve in Fig. S14 plots the ratio between the respective GC-FID areas of cyclohexanone oxime and Ph_2O vs. the relative amount of cyclohexanone oxime over Ph_2O.

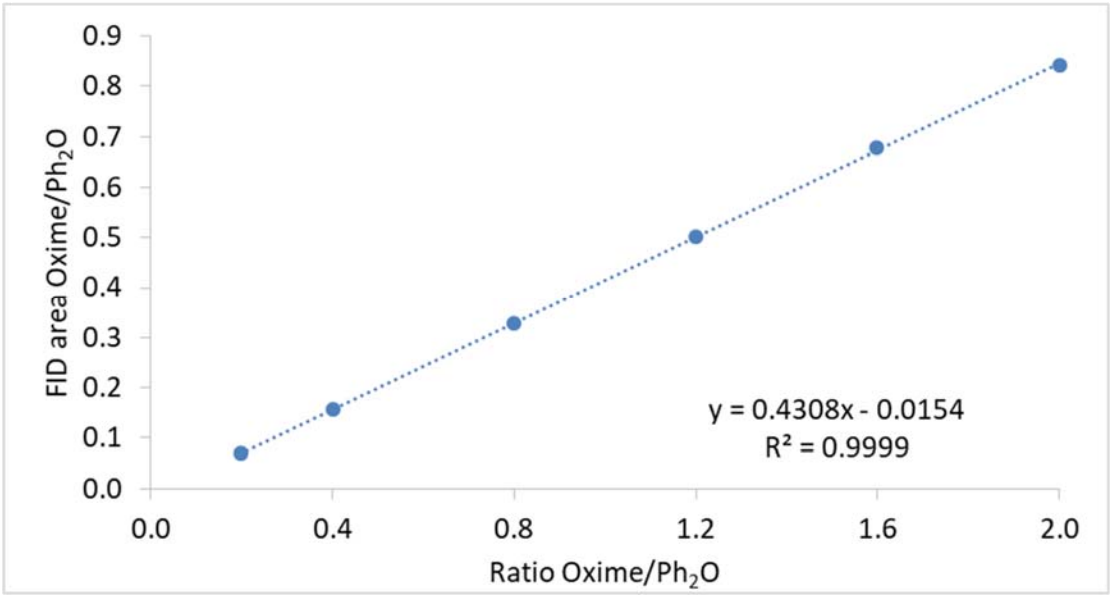

Fig. S14 GC-FID calibration for the quantification of cyclohexanone oxime using Ph_2O as internal standard.

The correlation between the excess of cyclohexane and cyclohexanone yield and selectivity, was investigated by varying the amount of substrate over nitrosyl chloride. The reaction products were quantified by GC-FID according to the general procedure and plotted in Fig. S15.

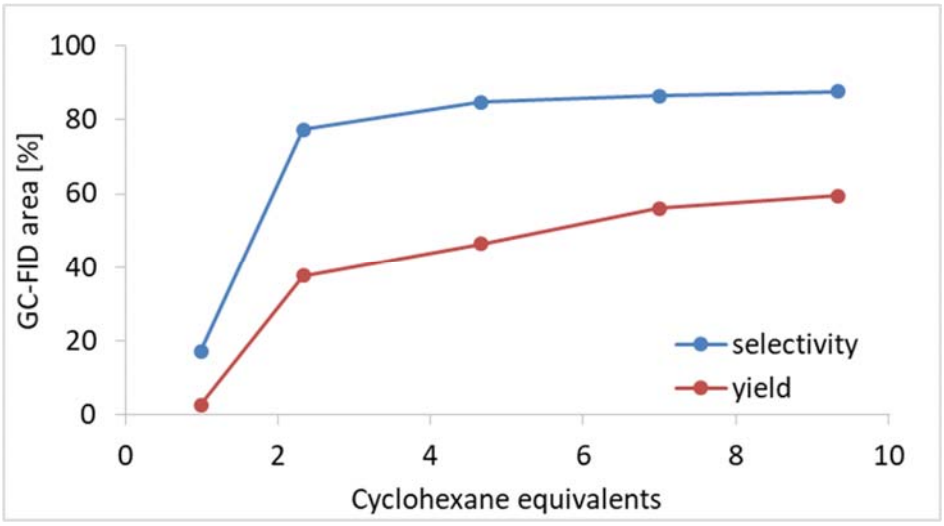

Fig. S15 Influence of cyclohexane equivalents.

2.4 Characterization of cyclohexanone oxime

The isolation of cyclohexanone oxime was confirmed by ^{1}H NMR, and further characterized using trichloroethylene as internal standard. To an NMR sample of the crude reaction product (10.0 mg) in DMSO-d_6, trichloroethylene (7.95 µL, 88.3 µmol) was added to determine the molecular weight of the isolated species. According to the integrated areas in Fig. S16, a molecular weight of 150.5 g/mol was calculated for the isolated product, which confirmed initial assumptions, that the product is isolated as monohydrochloride salt with a molecular weight of 149.6 g/mol under conditions employing NOCl for the photonitrosation of cyclohexane.

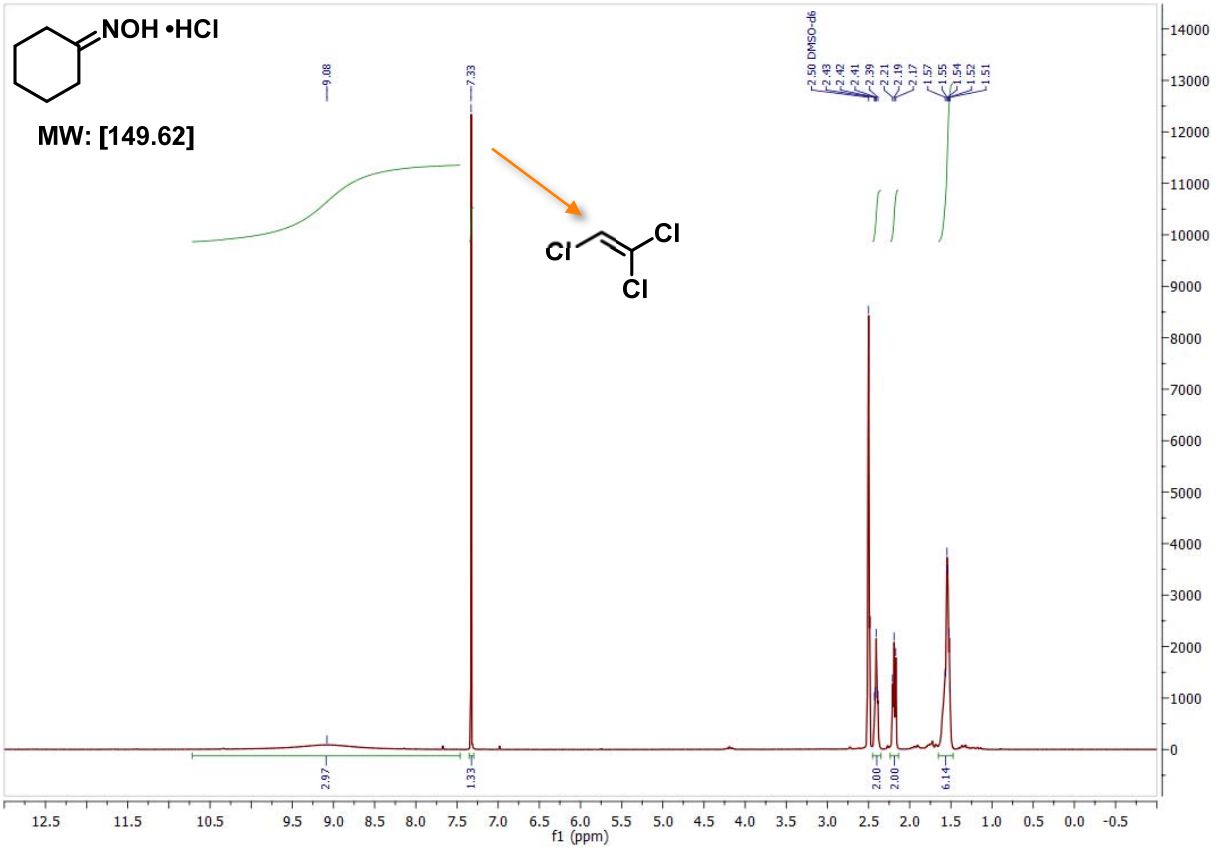

Fig. S16 ^{1}H NMR of the isolated cyclohexanone oxime using an internal standard.

3 References

S1 R. Weiß, K. Wagner and M. Hertel, *Chem. Ber.*, 1984, **117**, 1965–1972.

S2 E. K. Haub, A. C. Lizano and M. E. Noble, *Inorg. Chem.*, 1995, **34**, 1440–1444.

S3 M. Narendra Mallya, G. Nagendrappa, J. Shashidhara Prasad, M. . Sridhar, N. . Lokanath and N. . Begum, *Tetrahedron Lett.*, 2001, **42**, 2565–2568.

S4 US Pat., 9 181 177 B2, 2015.

4 NMR spectra